Two-point coherence of wave packets in turbulent jets

V. Jaunet and P. Jordan
Institut PPRIME, CNRS, Université de Poitiers, ENSMA,
86360 Chasseneuil-du-Poitou, France

A. V. G. Cavalieri
Divisão de Engenharia Aeronáutica, Instituto Tecnológico de Aeronáutica,
São José dos Campos, SP 12228-900, Brazil

(Received 4 February 2016; published 24 February 2017)

An experiment has been performed in order to provide support for wave-packet jet-noise modeling efforts. Recent work has shown that the nonlinear effects responsible for the two-point coherence of wave packets must be correctly accounted for if accurate sound prediction is to be achieved for subsonic turbulent jets. We therefore consider the same Mach 0.4 turbulent jet studied by Cavalieri *et al.* [Cavalieri *et al.*, J. Fluid Mech. **730**, 559 (2013)], but this time using two independent but synchronized, time-resolved stereo particle-image velocimetry systems. Each system can be moved independently, allowing simultaneous measurement of velocity in two, axially separated, crossflow planes, enabling eduction of the two-point coherence of wave packets. This and the associated length scales and phase speeds are studied and compared with those of the energy-containing turbulent eddies. The study illustrates how the two-point behavior of wave packets is fundamentally different from that of the more usually studied bulk two-point behavior, suggesting that sound-source modeling efforts should be reconsidered in the framework of wave packets. The study furthermore identifies two families of two-point-coherence behavior, respectively upstream and downstream of the end of the potential core, regions where linear theory is, respectively, successful and unsuccessful in predicting the axial evolution of wave-packets fluctuation energy.

DOI: 10.1103/PhysRevFluids.2.024604

I. INTRODUCTION

Coherent structures in turbulent jets have, for over 50 years, been considered important where jet noise is concerned. Since the earliest studies of Mollo-Christensen [1], the idea that these structures might be modeled as instability of the turbulent mean has been considered [2,3], leading to use of the term wave packet to describe this organized component of the flow motion. Since that time a large body of work has been devoted to studying and modeling wave packets (see [4] and references therein [5–15]).

Considerable progress has recently been made in the analysis, understanding, and modeling of jet noise source dynamics in the framework of hydrodynamic wave packets [4]. The success of linear theory in describing the wave-packet average structure up to the end of the potential core is remarkable. Farther downstream, however, discrepancies between theory and experiment are observed, and at low Strouhal numbers the discrepancies are considerable at all axial stations [16]. A second difficulty of linear theory lies in its failure to capture higher-order statistics, such as the two-point coherence. In the linear framework, wave packets have unit two-point coherence by construction. These shortcomings appear to underlie the failure of linear theory to obtain quantitatively accurate acoustic predictions for subsonic jets.

Previous attempts to explore the two-point structure of wave packets have been reported by Suzuki and Colonius [11], Reba *et al.* [17], and Breakey *et al.* [18] using measurements made in the near pressure field. Analyses (based on the two-point cross-spectral matrix of the axisymmetric pressure mode) show that while the first proper orthogonal decomposition (POD) mode captures

the structure of the average wave packet (computed using the linearized Navier-Stokes equations), higher-order modes are necessary to describe the wave-packet structure actually observed in the experiment downstream of the end of the potential core.

Computation of the acoustic pressure field based on the measured hydrodynamic near-field pressure, by means of a tailored Green's function, using both the raw and POD-filtered data, confirms the importance of the higher-order POD modes in correctly capturing acoustically important dynamics [18]: The use of one POD mode (which has unit coherence) to compute this acoustic extrapolation leads to a 25-dB underestimation (as does extrapolation of a linear solution obtained using the parabolized stability equations), while inclusion of the higher-order modes, which carry the missing coherence information, allows the missing 25 dB to be recovered. Baqui *et al.* [19] demonstrate how incorporating the two-point coherence measured by Breakey *et al.* [18] in their linear model leads to a correction of the acoustic predictions (a 25-dB deficit is again recovered).

The two-point pressure database of Breakey *et al.* [18] has been used by Piantanida *et al.* [20] and Sasaki *et al.* [21] to identify two-point, real-time, input-output models for closed-loop control; the latter paper considers such an input-output approach based on the parabolized stability equations. However, again, discrepancies in the downstream region and in the two-point coherence are manifest.

The above results motivate the present work. There is a need to probe the two-point statistics of wave packets, rather than the more usually studied energy containing eddies [22–26], in order to inform modeling improvements. An experiment dedicated to the extraction of this information has thus been performed. Dual-plane, time-resolved, stereoscopic particle-image velocimetry measurements are made in the same jet studied by Cavalieri *et al.* [16], from which the two-point coherence of the azimuthal Fourier modes of the velocity field is computed. This allows the extraction of coherence length scales and phase velocities of wave packets as a function of axial position and frequency. A comparison of the coherence length scales and phase velocities of wave packets to those of turbulent eddies reveals some important differences and, in particular, an absence of self-similarity that may be attributed to effects of nonlinearity that differ depending on the frequency and axial station considered.

A number of modeling remedies to the problems discussed above are explored [13,27–30]. All of these focus on the effects of nonlinearity on wave-packet dynamics and how best to incorporate these in models. As the two-point coherence is a key statistical signature of these nonlinear effects, the data and analysis provided by the work reported here are expected to provide guidance for these modeling efforts.

The experiment is described in Sec. II, followed by a validation in Sec. III. Section IV describes the contribution of wave packets to the two-point coherence function. Sections V and VI are dedicated to the presentation, analysis, and comparison of the two-point coherence and phase velocities of energy-containing eddies and wave packets. Closing comments are provided in Sec. VII.

II. EXPERIMENTAL SETUP

Experiments were conducted at the Bruit et Vent jet-noise facility of the Pprime Institute, Poitiers, France. The measurements were carried out at Mach number ($M = U_j/c$, where U_j is the jet velocity and c the ambient speed of sound) equal to 0.4 in isothermal condition. The nozzle diameter D was 0.05 m, giving a Reynolds number $\mathrm{Re} = \rho U D/\mu$ of 4.6×10^5. This is the same flow (same nozzle geometry and boundary layer trip) studied by Cavalieri *et al.* [16].

In order to enable decomposition of the flow field into azimuthal Fourier modes and subsequent extraction of the two-point structure of these, a dual-plane, time-resolved, stereoscopic particle-image velocimetry (PIV) system was used. The setup consisted of two synchronized time-resolved stereo PIV systems that could be moved independently, measuring instantaneous flow fields in the (r,θ) plane. The first system comprised two Photron SAZ cameras and a 527-nm 30-mJ Continuum MESA PIV laser, the second two Photron SA1 cameras and a 532-nm 6-mJ Continuum TERA PIV laser. All four cameras were equipped with 100-mm 2.8-aperture lenses so that the PIV images would cover the entire jet flow for axial positions up to $x/D = 5$. The angle formed by the optical axis of each

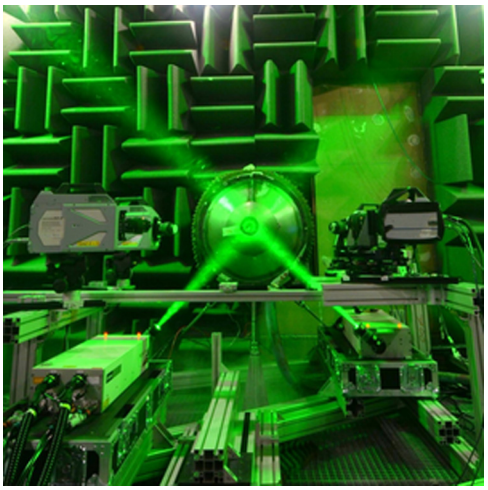

FIG. 1. Experimental setup.

lens and the laser light sheet plane was set to 30°, which was the maximum viewing angle possible given the optical access for measurement positions near the nozzle exit. This angle is sufficient for measurement errors between the three velocity components to remain in balance [31]. Scheimpflug adaptors were used, ensuring a correct focus on the complete field of view. The setup is shown in Fig. 1.

The arrangement of the two systems allows the two measurement planes to be either coplanar or axially separated. The axial positions of the measurement planes were $x_1 \in [1D,8D]$ and $x_2 \in [x_1,8D]$ in increments of $0.5D$, where x_1 refers to the axial position of the upstream system (S1) and x_2 to that of the downstream system (S2). For example, at a fixed position of S_1 at $x_1/D = 1$, the second system was successively positioned at $x_2/D = \{1,1.5,2,\ldots,8\}$, and for each (x_1,x_2) couple an acquisition was performed. Hence, a complete set of pairs of instantaneous velocity fields was collected and two-point information was then retrieved for varying reference points and separations. A schematic of the setup is shown in Fig. 2.

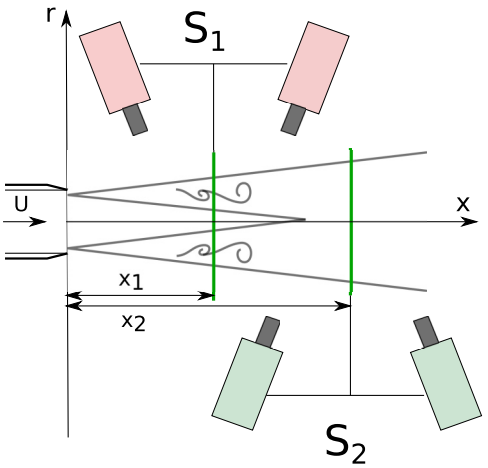

FIG. 2. Schematic of the experimental setup.

Both the jet flow and the surrounding air were seeded using pure glycerine smoke particles, whose diameters lie in the range 1–2 μm, sufficiently small to follow the velocity fluctuations of interest. Similarly to Schreyer *et al.* [32], we benefit from the fact that the two lasers have different wavelengths. With the help of a specifically chosen optical, 3-nm bandpass filter centered around each laser light wavelength, it was possible to distinguish the different laser light sheets when both measurement planes were in the field of view of the cameras. Moreover, as shown in Fig. 2, the cameras of each system were located opposite their laser source and the particle images were thus acquired in the forward-scatter mode for both systems. In this way, the light is backscattered by the laser of one system into the cameras of the other. This specific arrangement prevents any crosstalk between the images acquired by the two systems.

The laser-sheet thickness was set to 3 mm. The time between two laser pulses was set, accordingly, to 4 μs, corresponding to a maximum particle displacement of 5–6 pixels. This ensures a correct measurement dynamic range minimizing loss of particle pairs across the light sheet. The image acquisition was performed at 10 kHz (5000 PIV samples a second) at a resolution of 768×768 pixels on both systems, and for each acquisition, 19 414 image pairs were acquired, which represented in total 20 TB of images.

Particle-image velocimetry calculations were carried out using commercial software and a multipass iterative PIV algorithm [33]. The PIV interrogation area size was set to 32×32 pixels for the first pass and decreased to 16×16 pixels with an overlap of 50% between two neighboring interrogation areas. This led to a resolution of one vector every 0.85 mm and PIV vector fields containing 140×110 velocity vectors. Outliers were detected and replaced using the universal outlier detection technique [34]. The instantaneous velocity fields were interpolated onto a polar grid of 32 points in the radial direction and 64 in azimuth for $r/D < 0.8$ using a bicubic interpolation. The spatial resolution of the interpolated field has been chosen to match the original one in order to avoid any loss of information.

III. DATA VALIDATION

Given the technical difficulty of the experiment, thorough validation of the database is necessary. This section compares the data with that acquired a number of years ago by Cavalieri *et al.* [16] on what is nominally the same jet. The flow generation system and ducting have changed between the two experiments, but the convergent section, nozzle, and boundary layer trip are the same.

A. Comparison with previous measurements

Figure 3 shows a comparison of the mean and rms at $x/D = 2$. The current results are presented as an overlay of all the different measurement runs performed at this axial location. For the sake of visibility, not all the points are plotted and the data from the two PIV systems are plotted in a staggered manner.

Good agreement is obtained (Fig. 3) between previous and current measurements, between the two PIV systems and between successive runs, attesting to the high repeatability of the experiment. A slight difference is visible in the rms profiles inside the potential core of the jet, where the upstream system (S_1) shows higher values than the downstream one (S_2). This difference is confined to the potential core of the jet, i.e., for high velocity, leading us to postulate that the effect is due either to the laser pulse length of S_1, which is higher than that of S_2, or due to a difference in the light sheet thicknesses. Overly long laser pulses can lead to slightly blurred images and a correlation peak that is consequently broadened, leading to the addition of uncorrelated noise. An overly thin light sheet, on the other hand, can lead to the loss of particle pairs, which would also add noise to the displacement field [31,35]. Nevertheless, for measurement positions where the velocity is lower (for $r/D > 0.4$ in Fig. 3) both PIV systems agree very well.

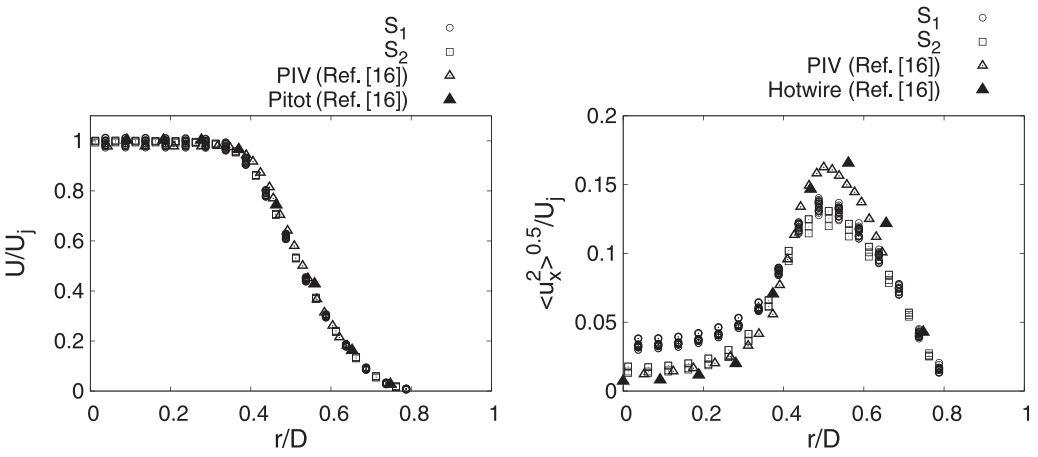

FIG. 3. Comparison of the current PIV results and data from Cavalieri *et al.* [16] at $x/D = 2$ for the mean (left) and rms (right) streamwise velocity profiles.

The current results appear to underpredict turbulence intensity measured by Cavalieri *et al.* [16] with PIV and a hot wire. This can be explained by the fact that Cavalieri *et al.* [16] used a higher magnification at this specific axial location.

B. Homogeneity

Figure 4 shows the mean Mach number profiles for several axial positions. For the sake of clarity, all the acquired positions are not presented here, but their results are comparable to those plotted in Fig. 4. It is clear from this figure that both PIV systems agree on the average Mach number at all measurement locations and for all runs performed.

The rms profiles are also shown in Fig. 4. As mentioned above, in the potential core of the jet the upstream system gives slightly higher fluctuation levels. Nevertheless, the higher measured value is about 2.5% on the centerline of the jet close to the nozzle, which is an acceptable signal-to-noise ratio (SNR) for a PIV measurement campaign. So, this actually demonstrates that the downstream system performed very well in terms of the SNR.

Beyond the end of the potential core ($x/D = 5$) and within the mixing layers the rms profiles provided by both systems collapse perfectly for all measurement locations and all acquisition runs. In addition to the demonstration of good repeatability of the experiment, this also shows that the alignment of the PIV systems was maintained during the entire data-acquisition process.

C. Wave packets in the velocity fields

In order to educe wave packets from the PIV data, the space-time-dependent velocity fluctuation $\mathbf{u}(x,r,\theta,t)$ is decomposed into Fourier modes in azimuth

$$\mathbf{u}(x,r,\theta,t) = \sum_m \tilde{\mathbf{u}}_m(x,r,t)e^{im\theta}, \tag{1}$$

where m is the azimuthal mode number and $\tilde{\mathbf{u}}_m$ the modal amplitude. In order to facilitate the discussion to follow, we reproduce in Fig. 5(a), using the current data set, the results of Cavalieri *et al.* [16], but over a broader range of axial stations. The fluctuation energy contained in the various azimuthal modes is shown as a function of axial position. Close to the nozzle exit the velocity fluctuations are dominated by high azimuthal wave number. The most energetic wave number decreases as we move downstream. As shown by Cavalieri *et al.* [16] and here in Fig. 5(b), the

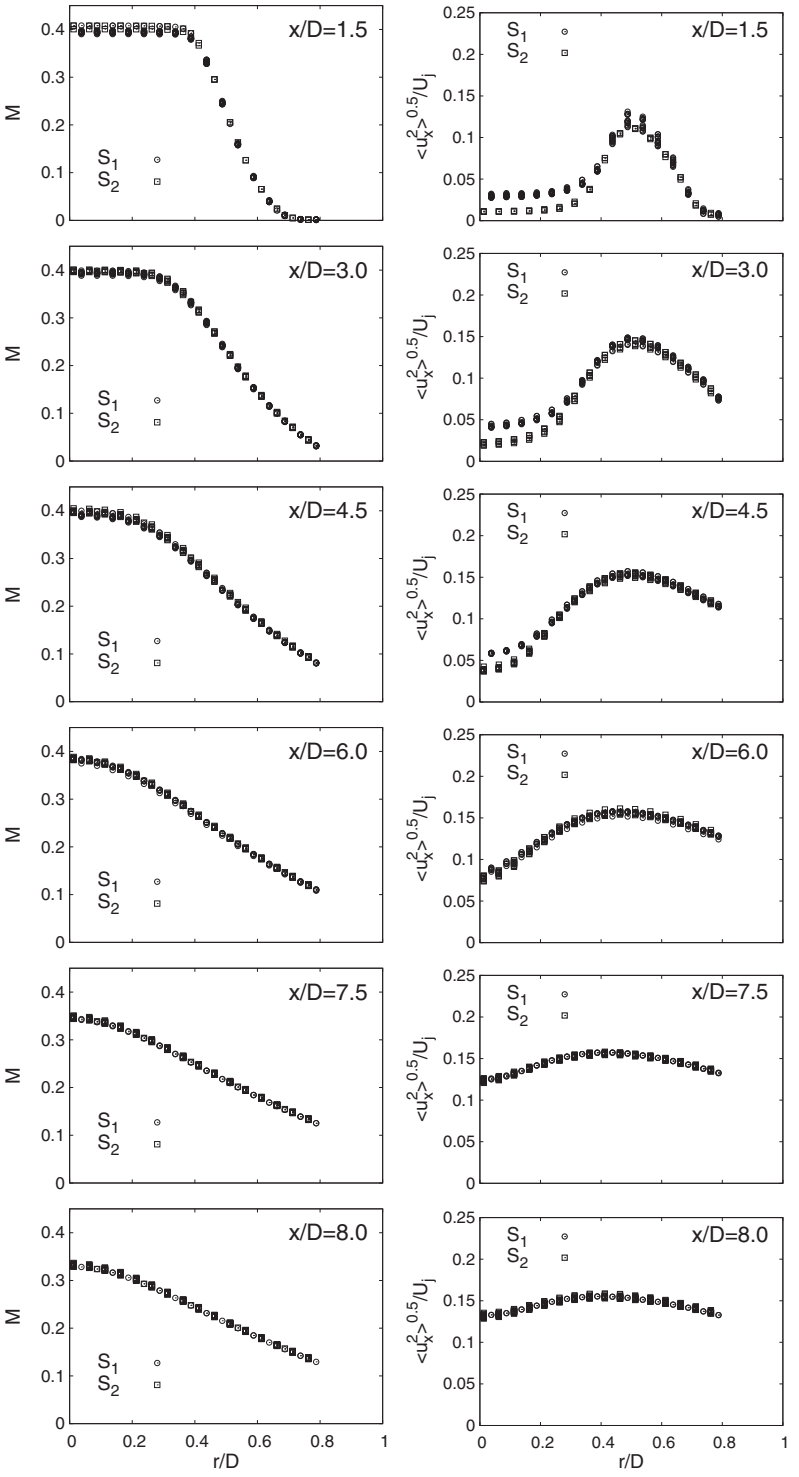

FIG. 4. Mean streamwise Mach number (left column) and turbulent intensity (right column) profiles at various axial locations.

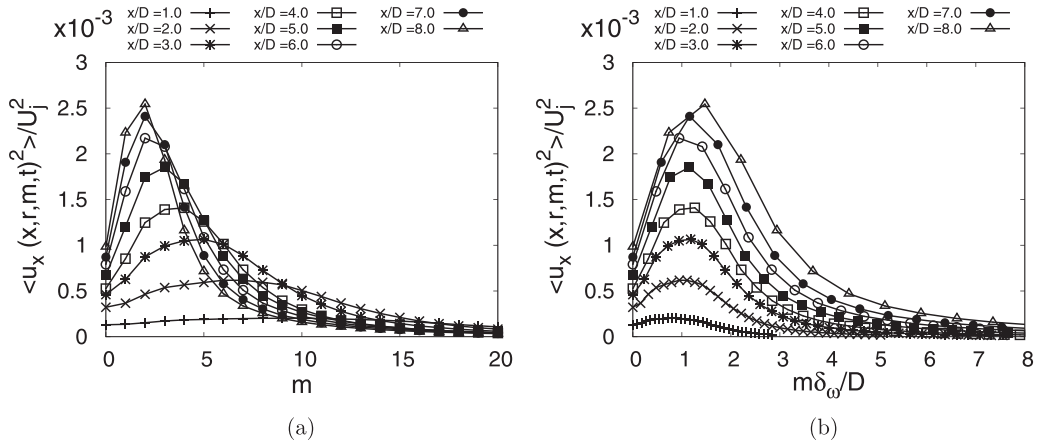

FIG. 5. Energy of the streamwise velocity fluctuation as a function of (a) the azimuthal mode number and (b) the mode number scaled with local vorticity thickness $\delta_\omega(x/D)$ for several axial positions in the jet at $r/D = 0.5$.

peak azimuthal wave number scales with a local integral turbulence scale (we use the vorticity thickness δ_ω).

The analysis to come involves comparisons of the two-point characteristics of these energetically dominant eddies with those of the less energetic, low azimuthal wave numbers (e.g., $m = 0,1,2$); these have been shown by numerous studies [11,14,16] to be in good agreement with modal solutions of the linearized Navier-Stokes equations. Both experimental results and modal solutions present a wave-packet shape. Therefore, in the following we will refer to "axisymmetric mode" and "wave packet" interchangeably when considering disturbances of azimuthal Fourier mode $m = 0$.

The time-varying azimuthal mode can be further processed to obtain its power spectral density (PSD)

$$\hat{\mathbf{u}}_{m,\omega}(x,r) = \int_{-\infty}^{+\infty} \langle \tilde{\mathbf{u}}_m(x,r,t)\tilde{\mathbf{u}}_m^*(x,r,t+\tau)\rangle e^{-i\omega\tau} d\tau, \tag{2}$$

where ω is the frequency, an asterisk denotes a complex conjugate, $\langle\cdot\rangle$ represent the averaging operator, and $\hat{\mathbf{u}}_{m,\omega}$ is the modal coefficient corresponding to the mode (m,ω). Equation (2) is the Fourier transform of the azimuthal mode autocorrelation function, and is technically evaluated using Welch's periodogram technique.

We compare in Fig. 6 the modal coefficients obtained with those obtained by Cavalieri *et al.* [16], for the axisymmetric wave packet $m = 0$ of the streamwise velocity fluctuation u_x, at several Strouhal numbers ($\mathrm{St} = fD/U_j$) measured at $x/D = 2.5$. The mode coefficients exhibit a typical wave-packet shape, with a kink in the amplitude at the jet lipline.

Note that the current results are presented as an overlay of all the available acquisitions at this axial position. It can be seen again that data from the various acquisitions collapse well. As observed in the previous sections, inside the potential core of the jet the fluctuation amplitudes obtained with S_1 are overestimated.

IV. TWO-POINT COHERENCE

As discussed in the Introduction, the two-point coherence is of fundamental importance in sound-source modeling. Numerous previous studies have explored this quantity or its time-delay-domain equivalent, the two-point correlation function. In these studies, two-point measurements are most often concentrated on the jet lipline, where turbulent kinetic energy is greatest. Such measurements comprise contributions from both energy-containing eddies and wave packets, but are dominated

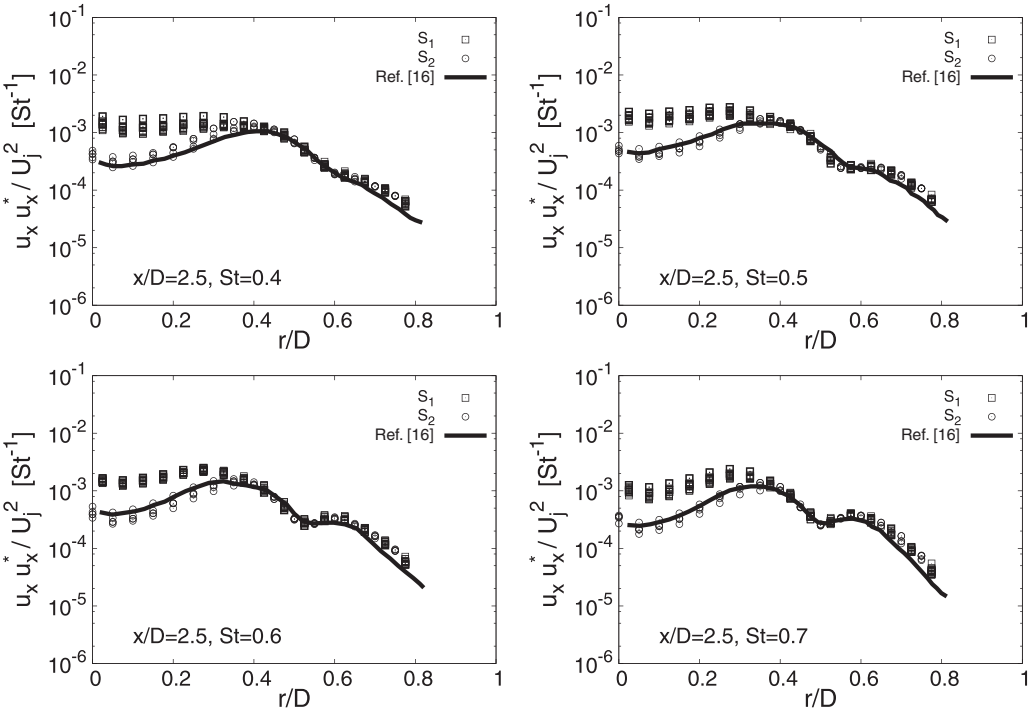

FIG. 6. Streamwise velocity fluctuation amplitude profiles at $x/D = 2.5$ for the axisymmetric mode and several Strouhal numbers.

by the former. It is today clear, at least for low-angle sound emission, that sound-source dynamics are dominated by wave packets, the axisymmetric of these being the most important. Two-point correlation or coherence functions computed using point measurements on the lipline therefore contain much redundant information where the sound-source dynamics are concerned. To get a sense of this we compute and compare the two-point coherence characteristics of energy-containing eddies and wave packets. For the latter, it is necessary to compute the coherence resolved into azimuthal Fourier modes; the coherence is thus calculated between two azimuthal rings in the flow, this being made possible by the measurement setup. Throughout the paper the term *two-point coherence* is used, but whenever this is calculated for a given azimuthal wave number, a two-ring calculation is of course implied.

The magnitude-squared coherence (MSC) function of the streamwise velocity component u_x is computed as a function of axial separation between two measurement points situated at $r/D = 0.5$. The two-point MSC function $\gamma(\mathbf{z}_1,\mathbf{z}_2,\omega)$ is defined as the normalized cross-spectral density (CSD)

$$\gamma^2(\mathbf{z}_1,\mathbf{z}_2,\omega) = \frac{|\langle\tilde{u}_\omega(\mathbf{z}_1)\tilde{u}^*_\omega(\mathbf{z}_2)\rangle|^2}{\langle|\tilde{u}_\omega(\mathbf{z}_1)|^2\rangle\langle|\tilde{u}_\omega(\mathbf{z}_2)|^2\rangle}, \tag{3}$$

where $\langle\cdot\rangle$ is the expectation operator, $\mathbf{z}$ the position vector, and $\tilde{u}_\omega(\mathbf{z})$ the Fourier coefficient of u_x at frequency ω.

The PSDs and CSDs were obtained using Welch's periodogram technique, with data blocks of 128 time samples overlapped by 50%. We ensured that for long separation distance an event measured at one position can be found in the signal of the second position by imposing a time shift corresponding to an overall convective speed of $0.6U_j$. Given the low sampling frequency of the PIV, this time shift corresponded to a maximum time shift of 20 time steps. The change of convective speed along the x axis (see Fig. 22) would only affect this value by one or two time steps, which is small compared

to the 128 time steps used in the blocks of data to compute the CSDs so that no artificial coherence decay are expected from the signal processing technique. This has been checked this by ensuring the consistence of the results obtained with a variety of different time shifts.

Since the jet is axisymmetric, the CSD and the MSC do not depend on θ but solely on $\Delta\theta = \theta_2 - \theta_1$ [19]. Further, since we want to focus on the axial structure of the coherence, the two-point MSC is considered for $\Delta\theta = 0$ and is averaged in the azimuthal direction to improve statistical convergence. The MSC is computed for all axial separations covered in the experiment, $\Delta x/D = x_2 - x_1$, and at a fixed radial position $r/D = 0.5$, chosen because it is a location of maximum turbulence intensity. Hence, for notational convenience the (r,θ) dependence will be dropped and the MSC will be denoted for the remainder of the paper by

$$\gamma^2(x,\Delta x,\omega) = \frac{1}{2\pi}\int_0^{2\pi} \gamma^2(x_1,x_2,r/D = 0.5,\Delta\theta = 0,\omega)d\theta. \tag{4}$$

As pointed out by Baqui *et al.* [19], the CSD can be expressed as the sum of its azimuthal Fourier coefficients, each of which depends only on the corresponding azimuthal mode of the velocity fluctuation:

$$C_\omega(x_1,x_2) = \sum_{m=-\infty}^{\infty} C_{\omega,m}(x_1,x_2) = \sum_{m=-\infty}^{\infty} \langle \tilde{u}_{\omega,m}(x_1)\tilde{u}^*_{\omega,m}(x_2)\rangle. \tag{5}$$

From Eq. (5) the MSC function can be expressed in terms of a sum of the azimuthal Fourier coefficients of the CSD. This allows us to define the cumulative coherence function

$$\Gamma^2_p(x_1,x_2,\omega) = \frac{\left|\sum_{m=-p}^{p}\langle \hat{u}_{\omega,m}(x_1)\hat{u}^*_{\omega,m}(x_2)\rangle\right|^2}{\langle|\tilde{u}_\omega(x_1)|^2\rangle\langle|\tilde{u}_\omega(x_2)|^2\rangle}, \tag{6}$$

which represents the contribution of the first p azimuthal modes to the overall two-point coherence. Figure 7 shows the function for different values of p and various Strouhal numbers. We note that the cumulative coherence function obtained using all the azimuthal modes is exactly equal to the standard two-point coherence function for all Strouhal numbers, as expected from the development of Baqui *et al.* [19]. The more interesting result, however, is that the first three azimuthal Fourier modes, which are associated with the wave packets most important for sound generation [4,36], contribute less than 10% to the complete two-point coherence.

From these observations it is tempting to conclude that the two-point coherence is dominated by high-order azimuthal modes, i.e., energy containing eddies (cf. Fig. 5). However, as the coherence is a sort of weighted average of the CSD of the individual azimuthal modes [see Eq. (5)], the cumulative coherence result in itself does not suffice for such a claim. The contribution of each of the azimuthal modes to the CSD is thus presented in Fig. 8. We clearly see that the CSD is dominated by azimuthal modes possessing most of the fluctuating energy (cf. Fig. 5) and that the axisymmetric mode has a very low CSD in comparison. In what follows we thus make a distinction between the bulk two-point coherence (which is underpinned by the energy-containing eddies) and that of the wave packets ($m = 0, \pm1, \pm2$).

The implications of the small wave-packet contribution to the bulk two-point coherence are considerable. In much previous source-modeling work [25,26,37–41] bulk two-point statistics (correlations and/or coherence) are considered. Functional forms used to model these are based on turbulence length scales, i.e., those dominated by energy-containing eddies. In light of the theoretical prediction [6,42], experimentally supported by the flow-acoustic correlations of Cavalieri *et al.* [16], that lower-order azimuthal modes are the most acoustically efficient, Fig. 7 demonstrates that bulk two-point statistics contain much acoustically redundant information. They are dominated by flow activity that is not acoustically matched.

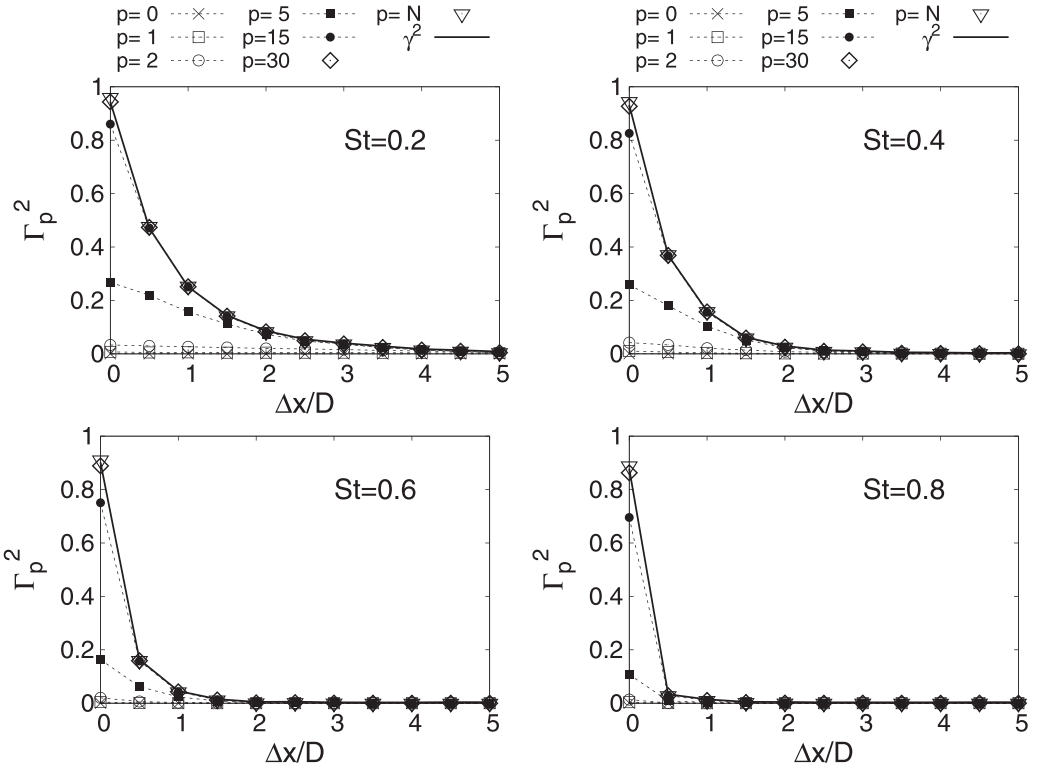

FIG. 7. Cumulative coherence function as a function of separation distance for various Strouhal numbers at $x/D = 3.0$ and $r/D = 0.5$.

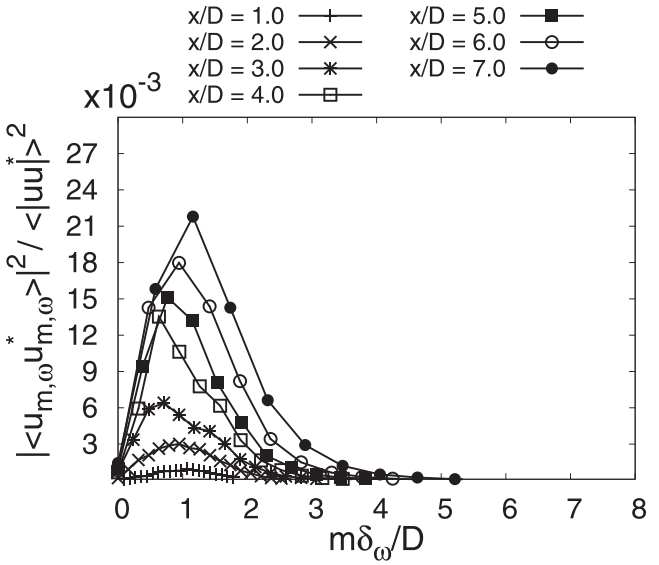

FIG. 8. Contribution of each azimuthal mode to the two-point CSD at St $= 0.3$ for $\Delta x/D = 0$, $r/D = 0.5$, and varying axial reference positions.

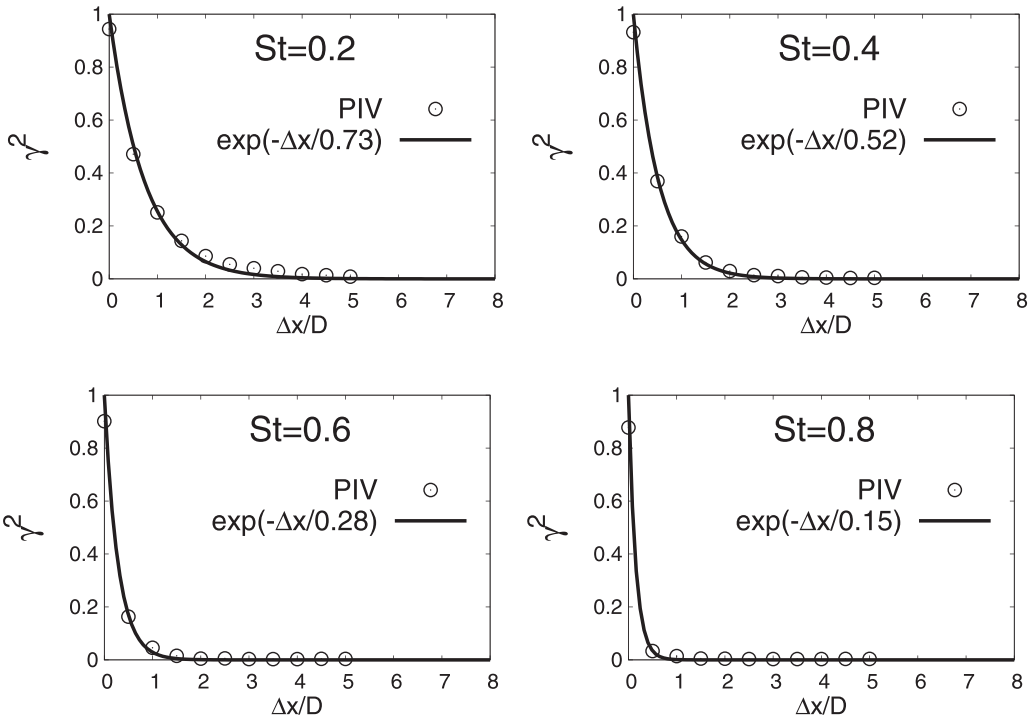

FIG. 9. Magnitude-squared coherence function of u_x at $x/D = 3.0$ and $r/D = 0.5$.

V. COHERENCE LENGTH SCALES

We explore here the coherence length scales of wave packets in more detail, comparing these systematically with those of the energy-containing eddies.

A. Energy-containing eddies

Figure 9 shows the MSC of u_x as a function of $\Delta x/D$, for a variety of Strouhal numbers, where the reference position is at $x/D = 3.0$ and $r/D = 0.5$. By definition the MSC should be unity for $\Delta x/D = 0$. We can see that the measured value is close to, but not equal to, one. This is due mainly to measurement noise, which is uncorrelated between the two systems, but slight alignment imperfections between the two PIV systems may also play a role. The MSC estimated from the measurement thus constitutes a slight underprediction. As it can be see in Fig. 9, the MSC decays with the separation distance, with a decay rate that is clearly a function of the Strouhal number. By fitting the decay rate with suitable functional forms, characteristic length scales can be extracted from the MSC as a function of axial position and frequency.

Kerhervé *et al.* [24] have shown that this decay can be described well by the product of Gaussian and exponential functions of the separation distance; Jordan *et al.* [43] and O'Hara *et al.* [44] proposed, in a similar spirit, for the two-point *correlation*, a function obtained by convolution of exponential and osculating parabola functions. In both cases the motivation was an accurate description of the function at small separations. The spatial resolution of the measurements reported here does not allow such finely tuned modeling of the function close to $\Delta x = 0$ and so the exponential function alone suffices to describe the global shape of the MSC. To identify the corresponding length scale the function $f(x) = \exp(-x/L)$ is fitted by a least-squares method to the data, for all St and x/D, and the space-frequency-dependent coherence length scale $L(\mathrm{St}, x/D)$ obtained. A similar procedure was used by Morris and Zaman [25]. The result is shown in Fig. 10.

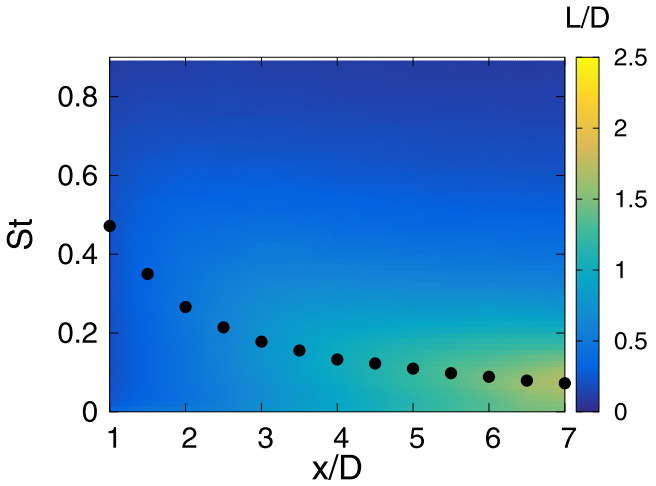

FIG. 10. Isocontours of coherence length of the energy-containing eddies. The black circles are located at $\mathrm{St} = 0.07 f \delta_\omega(x)/U_c$.

Two expected trends are evident from this figure. The first involves, for each axial position, a peak in the coherence length at some Strouhal number. The second is the evolution of this peak to lower St and the increase in associated length scale, as we move downstream. The trends are a reflection of the fact that the dominant (most energetic) turbulent eddies in the shear-layer scale with the local characteristics, for instance, the vorticity thickness; their peak frequency is expected to scale with U_c/δ_ω, where U_c is their convection velocity. The black circles in Fig. 10 show the equivalent local Strouhal number $\mathrm{St} = 0.07 f \delta_\omega(x)/U_c$ [22]. The fact that we see a larger coherence length at this characteristic frequency is an indication that these energetically dominant eddies are those that decohere least as they evolve downstream.

This situation is reflected by the collapse obtained in Fig. 11, where the coherence length scale $L(\mathrm{St}, x/D)$ is shown, nondimensionalized by the local vorticity thickness $\delta_\omega(x/D)$ and plotted against the shear-layer Strouhal number $\mathrm{St}_{\delta_\omega} = f\delta_\omega/U_c$, with $U_c = 0.6U_J$. The peak observed at $\mathrm{St}_{\delta_\omega} = 0.07$ is in good agreement with the frequency-dependent coherence length scales obtained by Kerhervé and Fitzpatrick [22] and Kerhervé *et al.* [24] using two-point laser Doppler velocimetry measurements in single- and dual-stream, heated, and isothermal jets. All of these studies indicate that the energy-containing turbulent eddies have spatial lifespans of about three times the local vorticity thickness and that they travel downstream at a roughly constant convection velocity $U_c = 0.6U_j$.

The key information to retain from this section is that the energetically dominant turbulent eddies scale with the local mixing-layer characteristics. This will be compared in the next section with the two-point structure of energetically weak but acoustically important wave packets.

B. Wave packets: Axisymmetric mode

The MSC of the axisymmetric mode $m = 0$ is plotted in Fig. 12 against the axial separation for various Strouhal numbers and for reference positions $x_0/D = 3.0$ at a fixed radial location $r/D = 0.42$. This radial location is chosen for several reasons. First, it is outside the potential core, therefore avoiding the region where the upstream system is affected by noise. Second, it is within the jet mixing layer but avoiding $r/D = 0.5$, where the streamwise velocity fluctuations of wave packets have low amplitude and experience a phase jump [16] (cf. Fig. 6). As this radial location differs from the one chosen for the energetic scales in the preceding section ($r/D = 0.5$), we present in Fig. 13 the comparison of the coherence decay of the energetic scales taken at $r/D = 0.42$ and $r/D = 0.5$. As can be seen, there are only minor changes of coherence decay between the two considered positions,

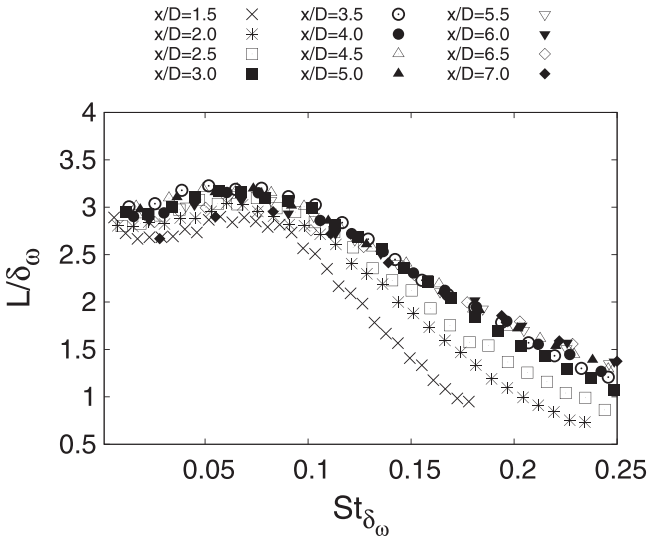

FIG. 11. Normalized coherence length as a function of the local Strouhal number $\mathrm{St}_\omega = f\delta_\omega/U_c$ for various x/D.

with a slightly faster decay when coherences are taken at 0.42. We have verified that the fact that we probe the wave packets and the energetic scales at different radial location does not change the conclusions that will be drawn in the following of this study.

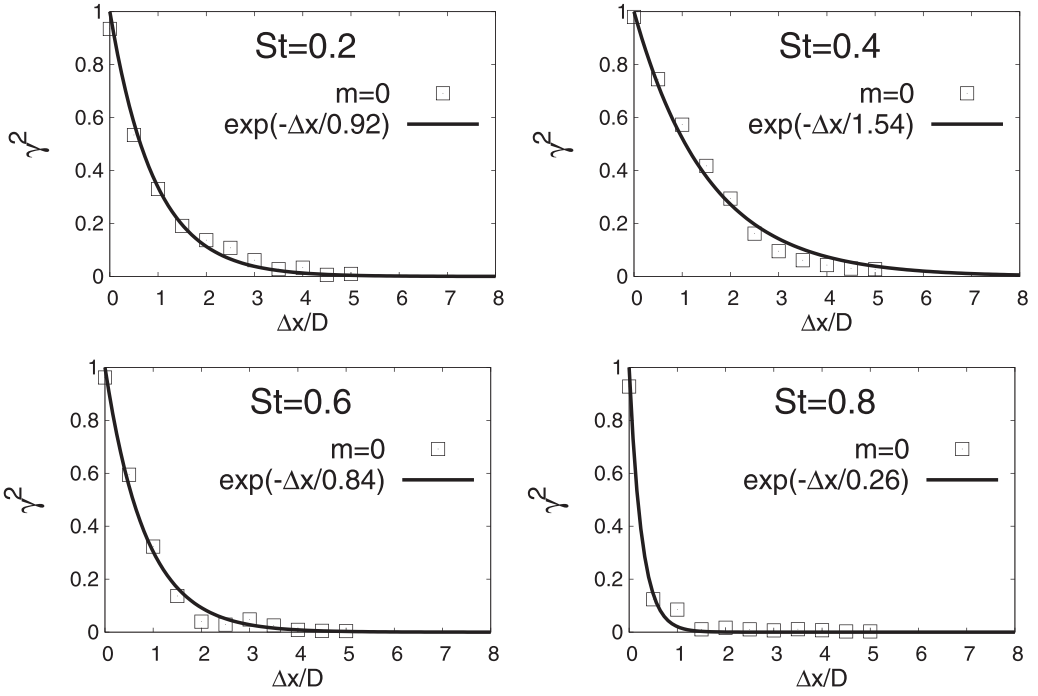

FIG. 12. Magnitude-squared coherence function of the axisymmetric mode $m = 0$ taken at $x/D = 3.0$ and $r/D = 0.42$.

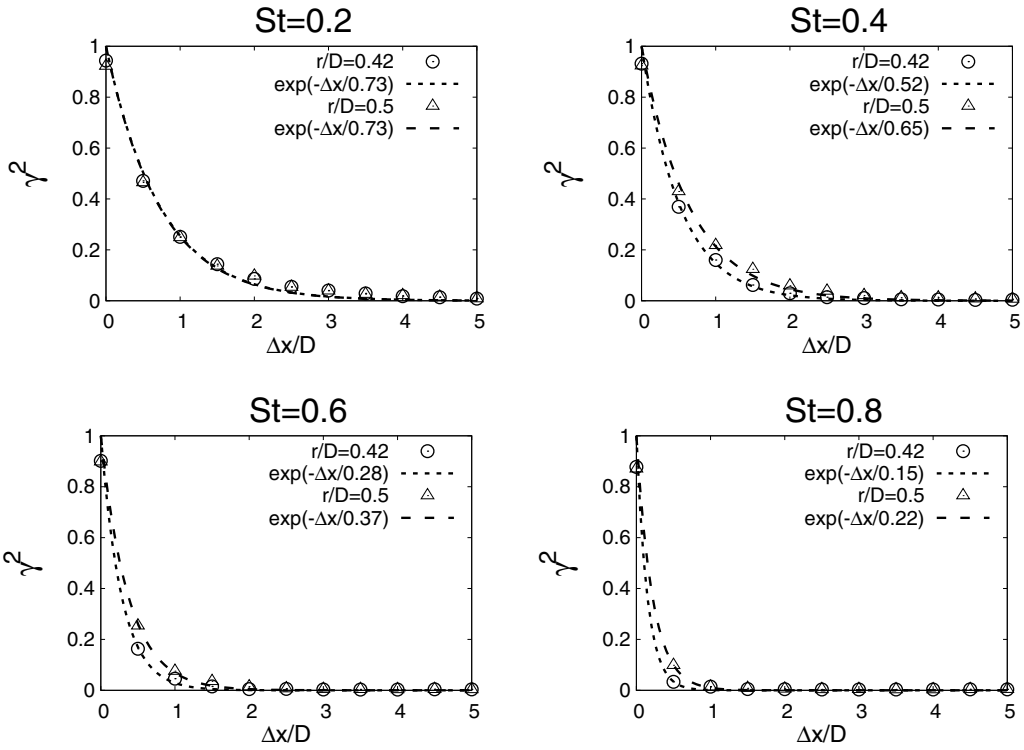

FIG. 13. Effect of radial location on the coherence decay of the energetic scales taken at $x/D = 3.0$ for various Strouhal numbers.

As for the energetic scales, the coherence function of the axisymmetric mode is fitted by means of a least-squares method with a decaying exponential function of a single parameter L, representing the coherence length of the wave packets. This is shown in Fig. 12.

The value of L that gives the best fit to the data is extracted for all axial reference positions and Strouhal numbers and is presented in Fig. 14. The map exhibits some important differences in comparison with Fig. 10. While there is again a peak at a preferred Strouhal number for each axial position that moves to lower St as we move downstream, reflecting the fact that high-frequency instabilities reach their maximum value farther upstream than their low-frequency counterparts, the peak value of L does not exhibit such a straightforward axial dependence.

We note that a similar observation can be made on examination of the results of Morris and Zaman [25]. Using two-point hot-wire measurements with the reference probe located at $(x/D,r/D) = (5,0.5)$ and at $(5,0)$, they inadvertently probed, respectively, the energetic turbulent eddies and the axisymmetric wave packet (symmetry considerations lead to only $m = 0$ components of the axial velocity fluctuations on the jet centerline). The authors noted differences between the two-point statistics observed at the two locations and, in particular, larger length scales for the centerline measurements. In what follows we propose a discussion and interpretation of this result.

A comparison of the coherence length scales of the energetic eddies and axisymmetric wave packet is given in Fig. 15. We clearly see that there exist x-St regions where the wave-packet coherence length scale is considerably larger than that of the energy-containing eddies (ECEs) [at $(x/D,\mathrm{St}) = (2,0.4)$, for instance]. On the other hand, elsewhere in the x-St domain, both the wave packet and the energetic eddies show similar coherence length scales. A space-frequency map of this difference $\Delta L = L_{\mathrm{WP}} - L_{\mathrm{ECE}}$ is shown in Fig. 16. Overlaid on the map is a template indicating the regions where linear stability models did (inside the polygon) and did not (outside the polygon)

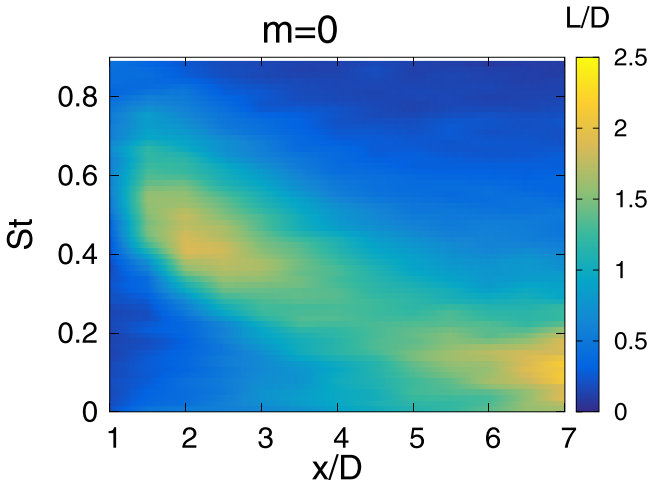

FIG. 14. Isocontours of coherence length of the axisymmetric mode $m = 0$.

successfully describe the dynamics of axisymmetric wave packets in this jet. The template is based on Figs. 15 and 26(b) of Cavalieri *et al.* [16]. A correspondence between the polygon template and ΔL is found: In x/D-St regions where linear models agree well with experiment (inside the polygon) the coherence length scales of wave packets differ significantly from those of the energy

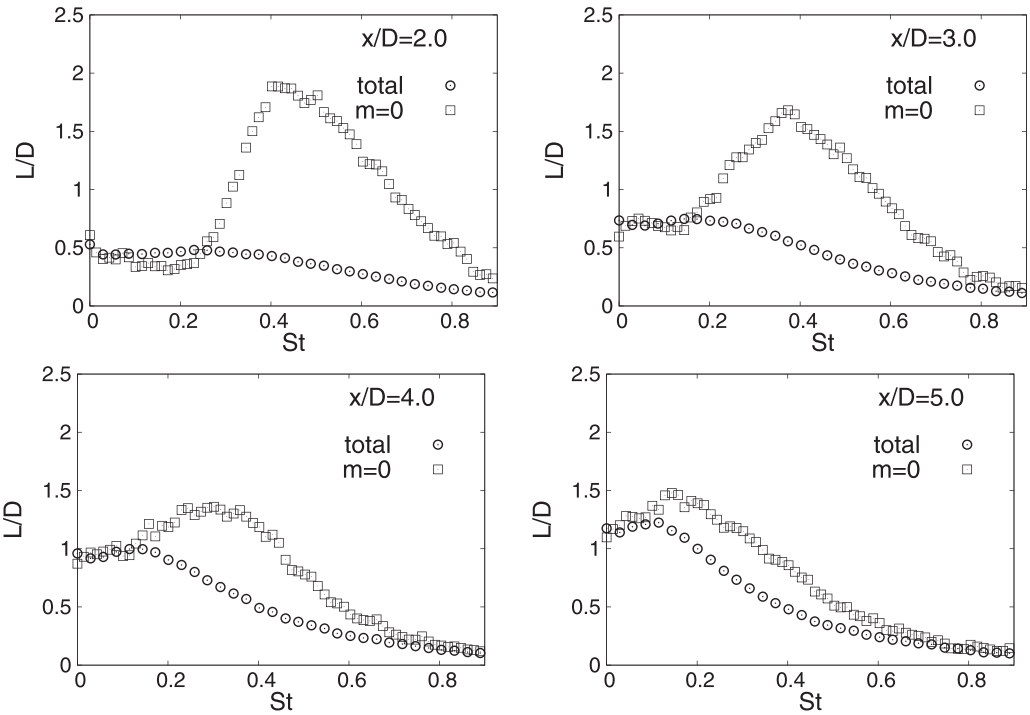

FIG. 15. Comparison of coherence length as a function of Strouhal number for various reference positions x/D.

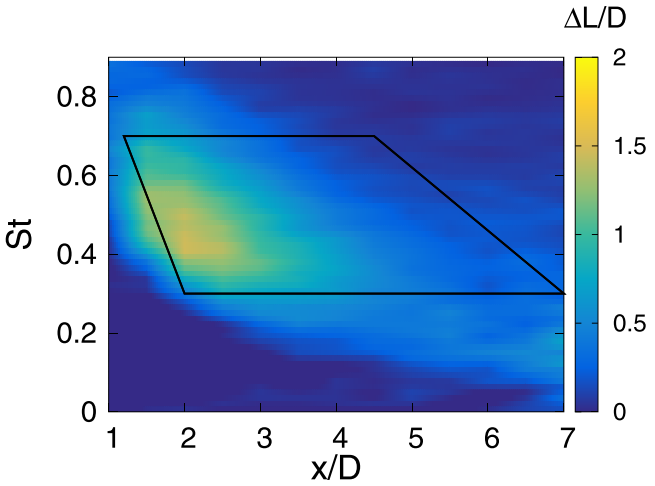

FIG. 16. Isocontours of $\Delta L = L_{\mathrm{WP}} - L_{\mathrm{ECE}}$. Inside the polygon is the portion of the [x,St] plane where linear stability theory is known to correctly describe the dynamic of the axisymmetric wave packet.

containing eddies, while in regions where the linear models fail (outside the polygon) the coherence length scales of wave packets and energy-containing eddies are similar.

This suggests two different scaling behaviors where wave packets are concerned, an idea tested in Figs. 17 and 18, where the wave-packet coherence length scales are nondimensionalized in two different ways. In Fig. 17 the jet exit diameter is used as a reference length scale and the convection velocity $U_c = 0.6U_j$ is used as a velocity scale. As can be seen, this scaling fails to collapse the data. Moreover, two families of curves can be identified depending on the axial station taken as the reference position; one family is observed upstream of the end of the potential core $x/D < 5$ (lines with symbols), while downstream $x/D > 5$ a second family is apparent.

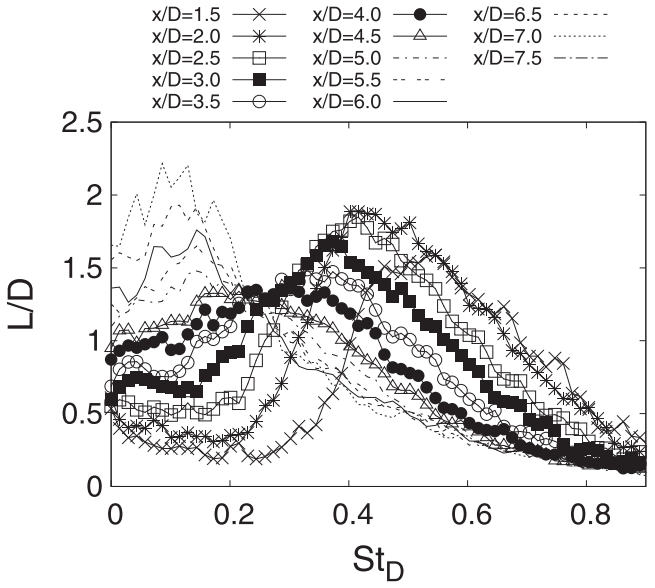

FIG. 17. Disparate wave-packet scalings. Two families of curves can be seen for $x/D < 5$ and $x/D > 5$.

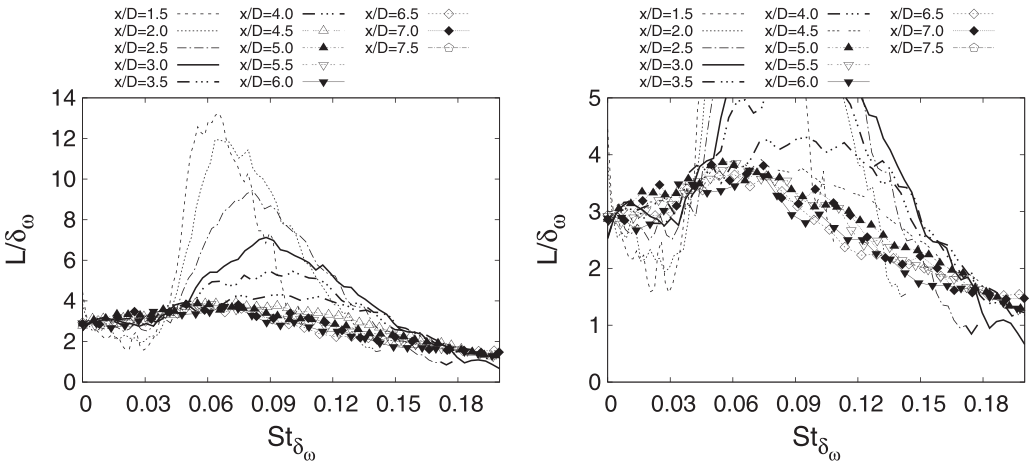

FIG. 18. (a) Disparate wave-packet scalings. For $x/D > 5$ and $\mathrm{St}_{\delta_\omega} < 0.04$ the local length scales collapse the coherence length but fail otherwise. (b) Close-up of (a).

In Fig. 18 the same scaling used for the energy-containing eddies is applied and found to collapse the data in the region downstream of the end of the potential core. We note that it is in this region of the jet that linear stability models disagree with experiments. By construction, linear stability solutions possess unit coherence. Hence, the fact that the axisymmetric mode decoheres rapidly in the region suggests that nonlinear interactions between wave packets and energy-containing eddies are significant in this region.

In the region upstream of the end of the potential core it was not possible to find a scaling that collapses the data. We can simply note that the wave-packet length scales in this region, where linear theory works well, are considerably larger (up to 12 times the vorticity thickness) than the local turbulence scales.

C. Asymmetry of the coherence function

Baqui *et al.* [19] used a Gaussian coherence function to model coherence decay. The two-point coherence was thus assumed to be symmetric about the reference position. Figure 19, which compares the two-point coherence of wave packets and energy-containing eddies considering spatial separations both upstream and downstream of the reference position ($x_0/D = 4$), shows that the wave-packet coherence function is asymmetric, decaying more rapidly in the downstream direction. This may be attributed to the fact that the flow is spatially developing and spreading as it evolves downstream, but could also be due to the increased importance of a nonlinear behavior of the wave packet in the downstream region. This asymmetric form will be important in determining the acoustic efficiency of wave packets; an analysis of this using model problems is beyond the scope of the present study. Papamoschou [45] has considered the asymmetry of the amplitude envelope of wave packets in his study, but not the asymmetry of their coherence.

We present in Fig. 20 the coherence functions taken at $x/D = 6$ for the same Strouhal numbers as in Fig. 19. This figure shows that the asymmetry of the wave packets is decreasing for high Strouhal numbers when considering downstream positions. This may be due to the fact that the higher-frequency wave packets at this position are beyond the point where the Kelvin-Helmholtz mode has become stable. Downstream of this position nonlinear and/or non-normal effects are believed to be more important and the wave-packet behavior changes accordingly. Further discussion of these mechanisms, which are being explored in a number of other studies (see, e.g., [28,46]), is beyond the scope of this paper.

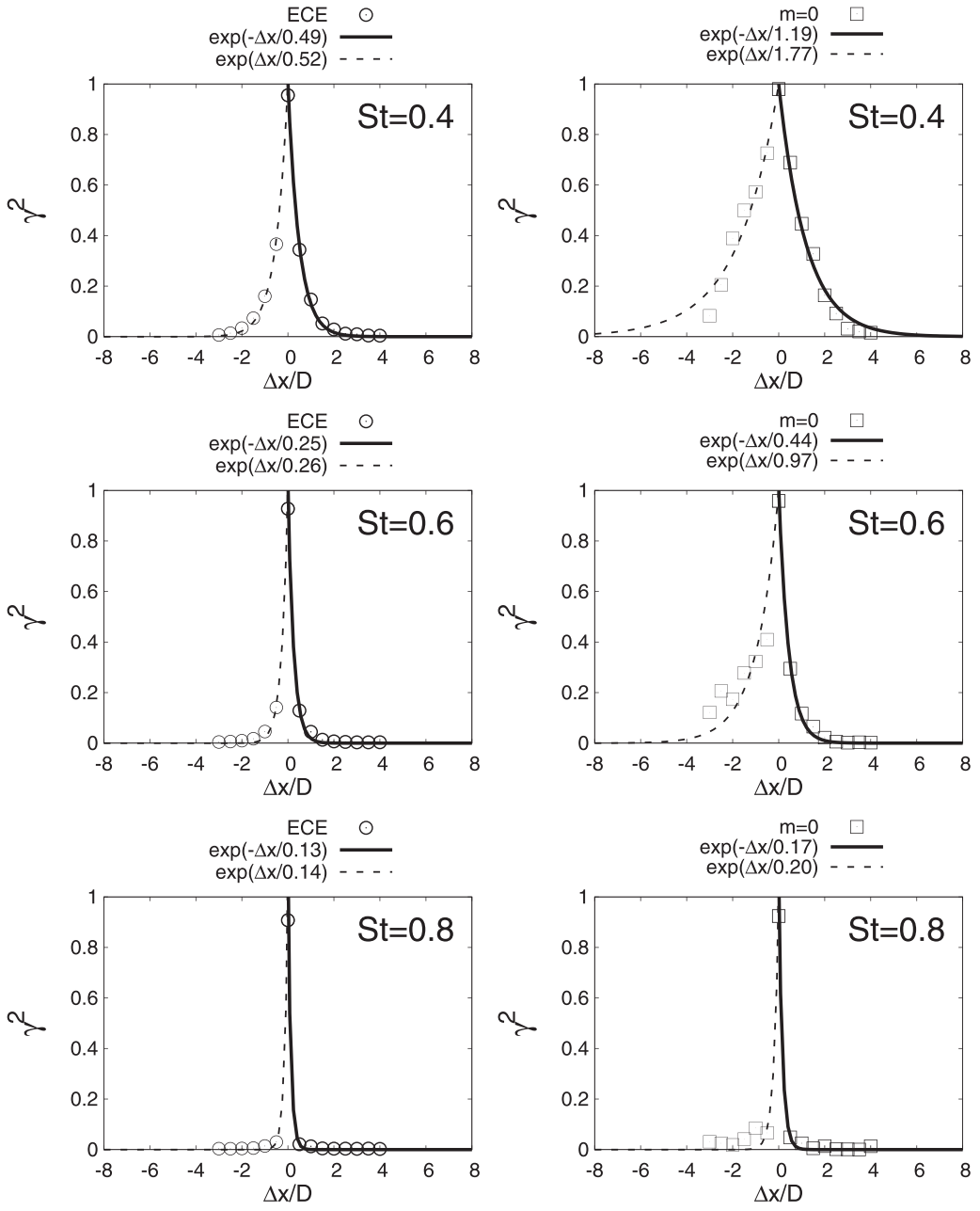

FIG. 19. Asymmetry of the coherence function at $x/D = 4$ for various Strouhal numbers. Energy-containing eddies are shown on the left and the axisymmetric mode $m = 0$ is shown on the right.

VI. PHASE VELOCITY

As demonstrated by Cavalieri and Agarwal [47], the coherence length of the statistical sources used in linear models is not the only parameter of importance with regard to sound radiation of subsonic jet flows. They considered a line source S, modeled in the frequency domain as a wave packet with Gaussian envelope of length L_w and a coherence length L_c, whose CSD between two

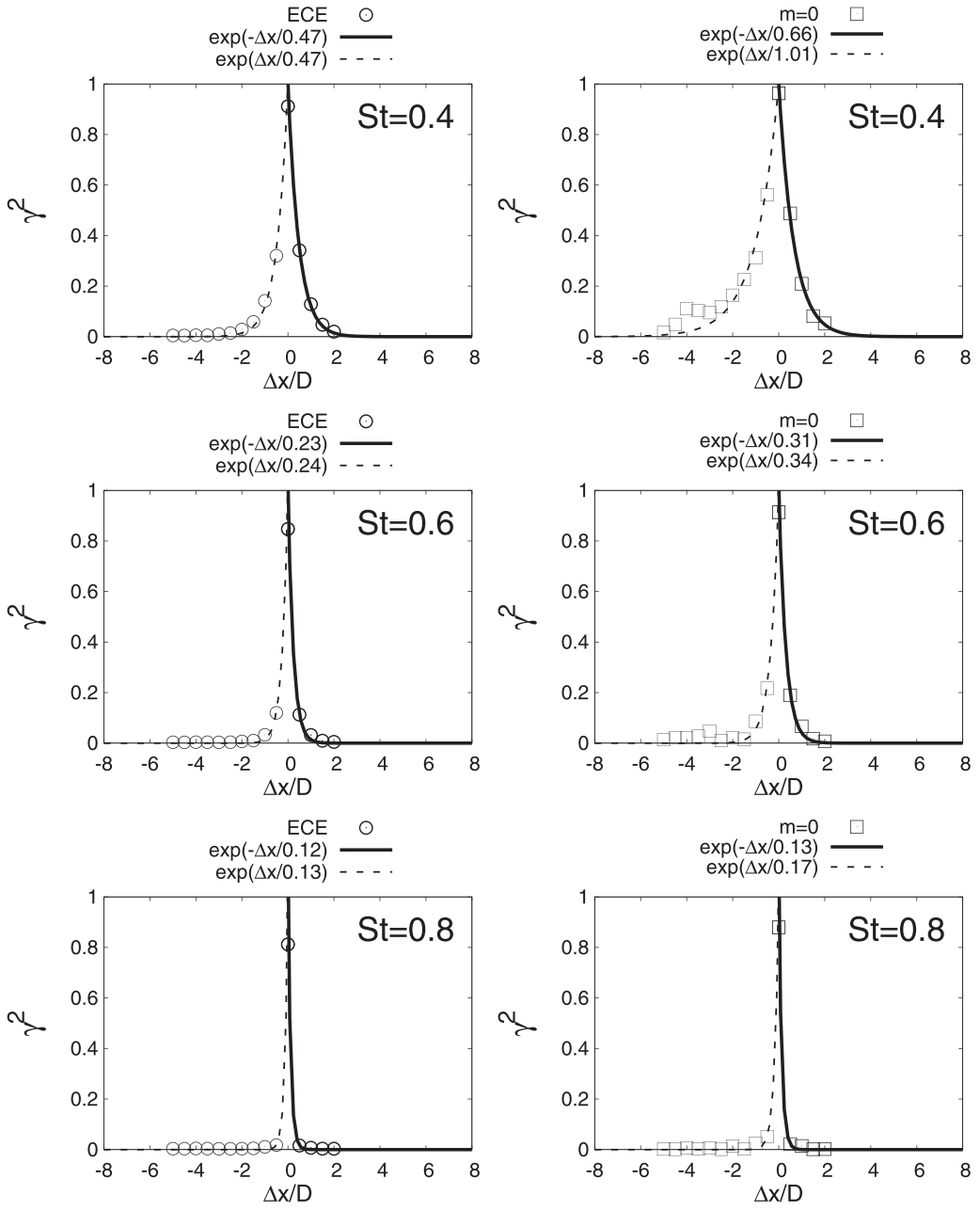

FIG. 20. Asymmetry of the coherence function at $x/D = 6$ for various Strouhal numbers. Energy-containing eddies are shown on the left and the axisymmetric mode $m = 0$ is shown on the right.

points y and z is given by

$$\langle S_\omega(y) S_\omega^*(z)\rangle = \exp\left(i\frac{\omega}{V_\phi}(y-z)\right)\exp\left(-\frac{y^2-z^2}{L_w^2}\right)\exp\left(-\frac{(y-z)^2}{L_c^2}\right), \tag{7}$$

where the $\exp(-i\omega t)$ term is not shown for the sake of clarity. The first exponential term represents the phase shift observed between the two points and V_ϕ is the corresponding phase velocity. Cavalieri

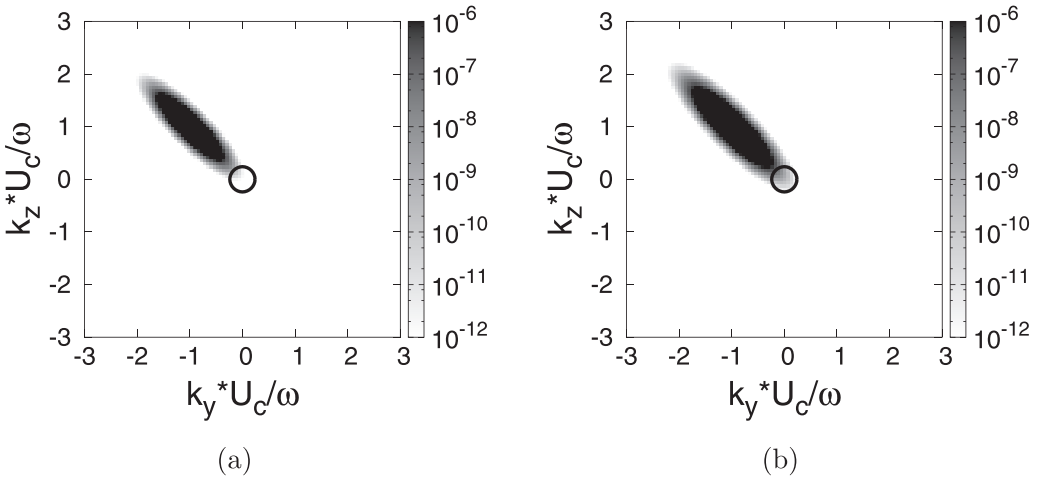

FIG. 21. Amplitude of the Fourier transform in space of the two-point line source CSD for (a) $V_\phi/U_j = 0.5$ and (b) $V_\phi/U_j = 0.6$. The source components with supersonic phase speed are located inside the black circle.

and Agarwal [47] showed that the far-field pressure PSD obtained with this source can be written as

$$\langle p(\mathbf{x},\omega)p^*(\mathbf{x},\omega)\rangle \simeq \frac{1}{8\pi x^2}\hat{S}_\omega(-k\cos\varphi, k\cos\varphi), \tag{8}$$

where k is the acoustic wave number, φ is angle from the observer to the downstream jet axis, and $\hat{S}_\omega$ is the double Fourier transform in space of the CSD (7),

$$\hat{S}_\omega(k_y,k_z) = \frac{L_m L_w}{2}\exp\left\{\frac{-L_m^2}{4}\left[\frac{(k_y+k_z)^2L_w^2}{L_c^2} + \left(\frac{\omega}{V_\phi}+k_y\right)^2 + \left(\frac{\omega}{V_\phi}-k_z\right)^2\right]\right\}, \tag{9}$$

where

$$L_m^2 = \frac{L_w^2 L_c^2}{2L_w^2 + L_c^2}. \tag{10}$$

Equation (8) shows that only wave numbers lower than k, i.e., the portion of the source with supersonic phase speed, contribute to the far-field radiation, which is expected from theory [47,48]. Hence, we see from Eq. (9) that for given coherence and wave-packet lengths, an increase in phase speed would displace the maximum amplitude of $\hat{S}_\omega$ towards the center of the wave-number plane, increasing the amplitude of the wavelength included in the region of supersonic phase speed wave numbers. This is illustrated in Fig. 21, where the amplitude of $\hat{S}$ is given for St = 0.4, with $L_w/D = 5.0$ and $L_c/D = 2.0$, and two different values of V_ϕ.

We compare in Fig. 22 the phase speeds of the axisymmetric wave packets with those of the energy-containing eddies (values obtained using two-point measurements). The phase speed is defined as

$$V_\phi = \frac{\omega}{k} = \omega\left(\frac{\partial\phi}{\partial x}\right)^{-1}, \tag{11}$$

where $\phi(x) = \arg[\hat{u}_{\omega,m}(x_1)\hat{u}^*_{\omega,m}(x_1)]$. Here $\frac{\partial\phi}{\partial x}$ was estimated by a linear regression of the measured phase shifts. The spatial resolution of the measurement in the axial direction does not allow us to compute correctly the phase derivative at high Strouhal number, therefore the results are only plotted for St $\leqslant 0.5$.

It is clear from Fig. 22 that the axisymmetric wave packet shows higher phase velocity than the energy-containing eddies for low Strouhal number St $\leqslant 0.3$, especially for $x/D \leqslant 5.0$. Interestingly,

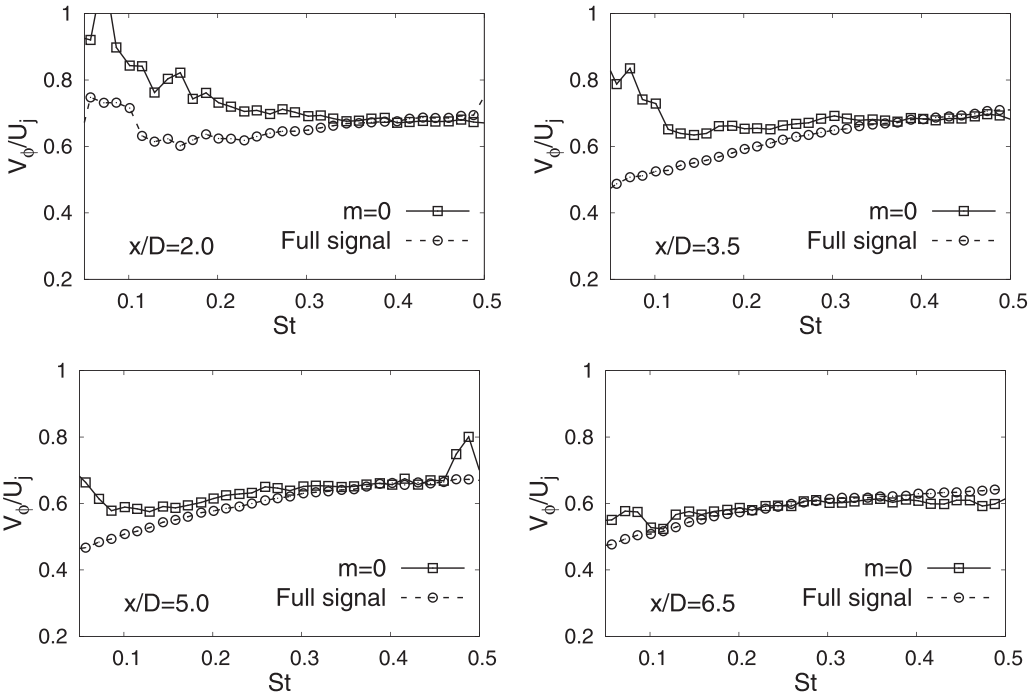

FIG. 22. Phase speed as a function of Strouhal number for various axial positions.

this range of Strouhal numbers and axial locations corresponds to the range where the wave packet and the energy-containing eddies show a similar coherence length (see Fig. 15). Elsewhere in the (x,St) domain the wave packet and turbulence show a similar phase speed. It is noticeable in Fig. 22 that the wave packets can propagate faster than the mean jet flow velocity, especially at locations close to the nozzle. This result is in agreement with linear stability theory and these fast waves were also experimentally observed by Bechert and Pfizenmaier [49] in a forced jet.

Hence, if wave packets do not exhibit a longer coherence length, their higher phase speed at low Strouhal numbers is likely to render them more efficient for far-field noise radiation. This effect is one that should be accounted for in jet-noise modeling.

VII. CONCLUSION AND PERSPECTIVES

Following the recent observation that linear wave-packet models of subsonic turbulent jets fail to get the sound field right on account of their incapacity to correctly model the two-point statistics, a dedicated experiment has been performed. This involved the synchronous implementation of two time-resolved stereo PIV systems, enabling measurement of the velocity in two axially separated crossplanes. The data were validated against previous hot-wire, pitot-tube, and single-plane PIV measurements. The two-point coherence of wave packets and energy-containing turbulent eddies were computed, analyzed, and compared and a number of characteristics important for sound-source modeling were thus identified.

By calculating a cumulative coherence function, it was shown that the acoustically important wave packets ($m = 0,1,2$) contribute less than 10% to the overall two-point coherence, suggesting that sound-source models based on this overall coherence comprise much redundant information. Space-frequency-dependent length scales were extracted and it was found that, while the length scales associated with the turbulent eddies show the expected behavior and scaling, in agreement

with previous work, those of the wave packets are fundamentally different in a number of important ways.

The wave-packet coherence length scales were found to be divided into two families, respectively upstream and downstream of the end of the potential core. In the latter region the wave-packet coherence-length-scale data exhibit a similarity behavior comparable to that of the energy-containing eddies, scaling with local turbulence quantities. Whereas upstream of the end of the potential core, in a region where wave-packet coherence length scales are an order of magnitude greater than the local turbulence scales, no similarity behavior is apparent.

These two families of coherence length scale can be compared with the results of linear wave-packet modeling, which was found to be most successful in the region upstream of the end of the potential core and whose failure downstream of this point is believed to be due to neglected nonlinear effects. Two final results, important for jet-noise modeling, are the observation of an asymmetry of the two-point wave-packet coherence in the region upstream of the end of the potential core and a higher phase velocity, in comparison to that of the energy-containing eddies, at peak noise frequencies.

The information provided by the study will be useful for the guidance of both kinematic and dynamic sound-source modeling efforts. Where the former are concerned, sound-source models of the kind previously studied by Cavalieri *et al.* [50] and Cavalieri and Agarwal [47] can now be further developed, account being taken for the various wave-packet characteristics that this study has identified. Hydrodynamic stability models that aim to incorporate the effects of nonlinearity [27,28,30] should be guided by the two-point coherence behavior we have observed and which they must ultimately capture if they are to correctly model the acoustic efficiency of wave packets.

ACKNOWLEDGMENT

The authors acknowledge support of the French National Research Agency (ANR) through the project COOLJAZZ.

[1] E. Mollo-Christensen, Measurements of near field pressure of subsonic jets, ASRL, TR 1009, 1963.
[2] D. G. Crighton and M. Gaster, Stability of slowly diverging jet flow, J. Fluid Mech. **77**, 397 (1976).
[3] K. A. Bishop, J. E. F. Williams, and W. Smith, On the noise sources of the unsuppressed high-speed jet, J. Fluid Mech. **50**, 21 (1971).
[4] P. Jordan and T. Colonius, Wave packets and turbulent jet noise, Annu. Rev. Fluid Mech. **45**, 173 (2013).
[5] E. Mollo-Christensen, Jet noise and shear flow instability seen from an experimenter's viewpoint, J. Appl. Mech. **34**, 1 (1967).
[6] A. Michalke and H. V. Fuchs, On turbulence and noise of an axisymmetric shear flow, J. Fluid Mech. **70**, 179 (1975).
[7] C. K. W. Tam and D. E. Burton, Sound generated by instability waves of supersonic flows. Part 2. Axisymmetric jets, J. Fluid Mech. **138**, 273 (1984).
[8] J. Cohen and I. Wygnanski, The evolution of instabilities in the axisymmetric jet. Part 1. The linear growth of disturbances near the nozzle, J. Fluid Mech. **176**, 191 (1987).
[9] R. A. Petersen and M. M. Samet, On the preferred mode of jet instability, J. Fluid Mech. **194**, 153 (1988).
[10] D. G. Crighton and P. Huerre, Shear-layer pressure fluctuations and superdirective acoustic sources, J. Fluid Mech. **220**, 355 (1990).
[11] T. Suzuki and T. Colonius, Instability waves in a subsonic round jet detected using a near-field phased microphone array, J. Fluid Mech. **565**, 197 (2006).
[12] J. Ryu, S. K. Lele, and K. Viswanathan, Investigation of the role of instability waves in jet noise radiation, *Proceedings of the 46th AIAA Aerospace Sciences Meeting, Reno, 2008* (AIAA, Reston, 2008), paper 2008-0026.

[13] N. D. Sandham and A. M. Salgado, Nonlinear interaction model of subsonic jet noise, Philos. Trans. R. Soc. London A **366**, 2745 (2008).
[14] K. Gudmundsson and T. Colonius, Instability wave models for the near-field fluctuations of turbulent jets, J. Fluid Mech. **689**, 97 (2011).
[15] X. Garnaud, L. Lesshafft, P. J. Schmid, and P. Huerre, The preferred mode of incompressible jets: linear frequency response analysis, J. Fluid Mech. **716**, 189 (2013).
[16] A. V. G. Cavalieri, D. Rodriguez, P. Jordan, T. Colonius, and Y. Gervais, Wavepackets in the velocity field of turbulent jets, J. Fluid Mech. **730**, 559 (2013).
[17] R. Reba, S. Narayanan, and T. Colonius, Wave-packet models for large-scale mixing noise, Int. J. Aeroacoust. **9**, 533 (2010).
[18] D. E. S. Breakey, P. Jordan, A. V. G. Cavalieri, O. Léon, M. Zhang, G. Lehnasch, and D. Rodríguez, Near-field wavepackets and the far-field sound of a subsonic jet, *Proceedings of the 19th AIAA/CEAS Aeroacoustics Conference and Exhibit, Berlin, 2013* (AIAA, Reston, 2013), paper 2013-2083.
[19] Y. B. Baqui, A. Agarwal, A. V. G. Cavalieri, and S. Sinayoko, A coherence-matched linear source mechanism for subsonic jet noise, J. Fluid Mech. **776**, 235 (2015).
[20] S. Piantanida, M. Le Rallic, P. Jordan, and T. Duriez, Armax system identification applied to a subsonic turbulent jet, *Proceedings of the 20th AIAA/CEAS Aeroacoustics Conference and Exhibit, Atlanta, 2014* (AIAA, Reston, 2014), paper 2014-3058.
[21] K. Sasaki, S. Piantanida, A. V. G. Cavalieri, and P. Jordan, Real-time modelling of wavepackets in turbulent jets, *Proceedings of the 21st AIAA/CEAS Aeroacoustics Conference and Exhibit, Dallas, 2015* (AIAA, Reston, 2015), paper 2015-2214.
[22] F. Kerhervé and J. Fitzpatrick, Spatio-temporal correlations for turbulent jet flows using the point reference global correlation (PRGC) technique, Proceedings of the 13th International Symposium on Applications of Laser Techniques to Fluid Mechanics, Lisbon, 2006 (unpublished).
[23] J. Panda, R. G. Seasholtz, and K. A. Elam, Investigation of noise sources in high-speed jets via correlation measurements, J. Fluid Mech. **537**, 349 (2005).
[24] F. Kerhervé, J. Fitzpatrick, and P. Jordan, The frequency dependence of jet turbulence for noise source modelling, J. Sound Vib. **296**, 209 (2006).
[25] P. J. Morris and K. B. M. Q. Zaman, Velocity measurements in jets with application to noise source modeling, J. Sound Vib. **329**, 394 (2010).
[26] C. D. Pokora and J. J. McGuirk, Stereo-PIV measurements of spatio-temporal turbulence correlations in an axisymmetric jet, J. Fluid. Mech. **778**, 216 (2015).
[27] P. Jordan, T. Colonius, G. A. Bres, M. Zhang, A. Towne, and S. Lele, Modeling intermittent wavepackets and their radiated sound in a turbulent jet, *Studying Turbulence Using Numerical Simulation Databases - XV*, Center for Turbulence Research Proceedings of the 2014 Summer Program (Stanford University Press, Stanford, 2014).
[28] G. Tissot, M. Zhang, F. C. Lajús, A. V. G. Cavalieri, and P. Jordan, Sensitivity of wavepackets in jets to nonlinear effects: the role of the critical layer, J. Fluid Mech. **811**, 95 (2017).
[29] M. R. Malik and C.-L. Chang, Nonparallel and nonlinear stability of supersonic jet flow, Comput. Fluids **29**, 327 (2000).
[30] A. Towne, T. Colonius, P. Jordan, A. V. G. Cavalieri, and G. Brès, Stochastic and nonlinear forcing of wavepackets in a Mach 0.9 jet, *Proceedings of the 21st AIAA/CEAS Aeroacoustics Conference and Exhibit, Dallas, 2015* (AIAA, Reston, 2015), paper 2015-2217.
[31] A. K. Prasad, Stereoscopic particle image velocimetry, Exp. Fluids **29**, 103 (2000).
[32] A.-M. Schreyer, J.-J. Lasserre, and P. Dupont, Development of a dual-PIV system for high-speed flow applications, Exp. Fluids **56**, 187 (2015).
[33] F. Scarano, Iterative image deformation methods in PIV, Meas. Sci. Technol. **13**, R1 (2002).
[34] J. Westerweel and F. Scarano, Universal outlier detection for PIV data, Exp. Fluids **39**, 1096 (2005).
[35] C. Willert, Stereoscopic digital particle image velocimetry for application in wind tunnel flows, Meas. Sci. Technol. **8**, 1465 (1997).
[36] A. V. G. Cavalieri, P. Jordan, T. Colonius, and Y. Gervais, Axisymmetric superdirectivity in subsonic jets, J. Fluid Mech. **704**, 388 (2012).

[37] R. H. Self, Jet noise prediction using the Lighthill acoustic analogy, J. Sound Vib. **275**, 757 (2004).
[38] J. B. Freund, Noise source turbulence statistics and the noise from a Mach 0.9 jet, Phys. Fluids **15**, 1788 (2003).
[39] W. J. Devenport, C. Muthanna, and R. M. S. Clegg, Two-point descriptions of wake turbulence with application to noise prediction, AIAA J. **39**, 2302 (2001).
[40] P. Jordan and Y. Gervais, Modelling self and shear noise mechanisms in inhomogeneous, anisotropic turbulence, J. Sound Vib. **279**, 529 (2005).
[41] F. Kerhervé, P. Jordan, Y. Gervais, J.-C. Valière, and P. Braud, Two-point laser Doppler velocimetry measurements in a Mach 1.2 cold supersonic jet for statistical aeroacoustic source model, Exp. Fluids **37**, 419 (2004).
[42] A. Michalke, Some remarks on source coherence affecting jet noise, J. Sound Vib. **87**, 1 (1983).
[43] P. Jordan, R. Wells, Y. Gervais, and J. Delville, Optimisation of correlation function models for statistical aeroacoustic noise prediction, Proceedings of the CFA/DAGA 2004 Acoustics Conference, Strasbourg, 2004 (unpublished).
[44] D. O'Hara, N. Andersson, P. Jordan, M. Billson, L. Eriksson, and L. Davidson, A hybrid analysis methodology for improved accuracy in low cost jet noise modelling, *33rd International Congress and Exposition on Noise Control Engineering* (Internoise, San Francisco, 2004).
[45] D. Papamoschou, Wavepacket modeling of the jet noise source, *Proceedings of the 17th AIAA/CEAS Aeroacoustics Conference (32nd AIAA Aeroacoustics Conference)* (AIAA, Reston, 2011).
[46] M. Zhang, Linear and non-linear waves in subsonic turbulent jets, Ph.D. thesis, University of Poitiers, 2016.
[47] A. V. G. Cavalieri and A. Agarwal, Coherence decay and its impact on sound radiation by wavepackets, J. Fluid Mech. **748**, 399 (2014).
[48] D. G. Crighton, Basic principles of aerodynamic noise generation, Prog. Aerosp. Sci. **16**, 31 (1975).
[49] D. Bechert and E. Pfizenmaier, On wavelike perturbations in a free jet traveling faster than the mean flow in the jet, J. Fluid Mech. **72**, 341 (1975).
[50] A. V. G. Cavalieri, P. Jordan, A. Agarwal, and Y. Gervais, Jittering wave-packet models for subsonic jet noise, J. Sound Vib. **330**, 4474 (2011).